MATERIALS CHEMISTRY
FRONTIERS

RESEARCH ARTICLE

View Article Online
View Journal | View Issue



Cite this: *Mater. Chem. Front.*, 2023, **7**, 2860

# Panchromatic luminescent D–π–A benzothiazoles with different π-bridging modulation: design, synthesis and application in WLED devices†

Yuwei Song, Yue He, Lai Hu, Qian Cheng, Zhiyuan Chen, Rui Liu,* Senqiang Zhu* and Hongjun Zhu

White light-emitting diodes (WLEDs) are gradually replacing traditional lighting devices and are becoming a mainstream photosource, as they have advantages of low energy consumption and high efficiency. However, a higher brightness and color purity are still required for the development of WLEDs. In this work, we have constructed donor (D)–π–acceptor (A)-type fluorescent small molecules using simple benzothiazole and dimethylamine as electron donor/acceptor groups, respectively. Six compounds with full-color luminescence have been obtained by introducing benzene, thiophene, and C=C double-bond units to modulate the π-bridge length. These six compounds covered the entire visible spectrum, not only in solution, but also in the aggregation state. Moreover, most of the compounds had a high luminescence efficiency. The fluorescence quantum yields of **PLB2** and **PLB3** are even close to 1.0. We have used **PLB1**, **PLB3**, **PLB4**, and **PLB6**, which display good luminescence properties in both the aggregated and dispersed states, to fabricate LEDs. Two **PLB4**-based WLEDs have also been prepared, designated as warm-white and cool-white devices. Their luminous efficiencies were measured as 115.81 lm $W^{-1}$ and 95.31 lm $W^{-1}$ and their color rendering indices (CRI) were evaluated as 60 and 80, respectively. These key parameters exceeded those of commercial WLEDs. In addition, four compounds have been utilized to prepare blue, green, yellow, and near-infrared LEDs, all of which surpassed the performances of existing commercial LEDs.

Received 23rd February 2023,
Accepted 30th March 2023

DOI: 10.1039/d3qm00189j

rsc.li/frontiers-materials



## Introduction

According to the United States Department of Energy, lighting consumes 15% of the world's energy and accounts for 5% of the world's greenhouse gas emissions.[1] Light-emitting diodes (LEDs) and organic LEDs (OLEDs) have attracted wide attention by virtue of their advantages of low energy consumption and high efficiency.[2–4] Thus, white LEDs (WLEDs) are gradually replacing traditional lighting devices, such as incandescent and fluorescent lamps.[5–7] In general, white light emission is obtained by combining the three primary colors (red, green, and blue) or two complementary colors (red-cyan, green-magenta, and blue-yellow/orange).[8] The strategy of using a combination of three primary colors seems to be the easiest means of obtaining standard white light. However, the components can interfere with each other at high operating voltage, destabilizing the emission spectrum, and thereby affecting the efficiency of the device.[9,10] Existing commercial WLED products mainly contain a blue LED as the primary light source, together with a light-conversion material to convert blue light into complementary yellow light.[11] One of the most striking examples is the WLED prepared by incorporating a yellow phosphor ($Y_3Al_5O_{12}$:$Ce^{3+}$) in blue chips.[12] The simplest and most effective method for preparing WLEDs is to coat sample films or gels on the surfaces of commercial blue LED chips/bulbs.[13] An efficient yellow/orange luminescent material is essential for this preparation strategy.

Small organic molecules, which are simple to synthesize and easy to regulate, are undoubtedly the best choice for light-conversion materials in WLEDs. Moreover, these materials have been widely used as color conversion layers in organic WLEDs (WOLEDs).[14–16] However, higher brightness and color purity are still issues that need to be addressed for these WLEDs.[17] It is easier to screen for materials required for higher color purity WLEDs among compounds with tunable full-color

*School of Chemistry and Molecular Engineering, Nanjing Tech University, Nanjing 211816, China. E-mail: zhusenqiang1993@njtech.edu.cn, rui.liu@njtech.edu.cn*

† Electronic supplementary information (ESI) available: Experimental details and additional characterization and analysis of **PLB1–PLB6**. CCDC 2232818 (for **PLB1**), 2232819 (for **PLB2**), 2232820 (for **PLB3**), and 2232821 (for **PLB4**). For ESI and crystallographic data in CIF or other electronic format see DOI: https://doi.org/10.1039/d3qm00189j

 

luminescence.[18–20] In recent years, researchers have been working with D–π–A-type molecules to fabricate materials with panchromatic luminescence.[21–23] A common strategy is to use different electron donor/acceptor groups to modify the material, such that its emissions are red-shifted or blue-shifted.[24–26] Moreover, π-bridge modulation is also an effective strategy and permits the production of materials with high quantum yields.[27] The introduction of polymethylene chains as π-bridges can modulate the luminescence color to the near-infrared region.[28,29] To maintain the stability of the material, a benzene or thiophene unit is often used in combination with polymethylene chains to build π-bridges.[30,31] Such materials have been widely reported for applications in LEDs,[32–34] fluorescent probes,[35–37] and bioimaging.[38–40]

Benzothiazole is a chromophore with easily tunable luminescence properties.[41–43] In our previous work, materials of this class were shown to be suitable for application in WLEDs.[44] For this work, we have selected simple benzothiazole and dimethylamine as electron donor/acceptor groups, respectively, to construct D–π–A-type fluorescent small molecules. Benzene, thiophene, and C=C double-bond units have been introduced to regulate the π-bridge conjugates. In this way, we designed and synthesized six fluorescent small molecules (Scheme 1). Their absorption and emission wavelengths were progressively red-shifted with increasing length of the π-bridge. These six compounds covered the entire visible spectrum, not only in solution, but also in the solid state. Notably, most of these compounds had high luminescence efficiency. The fluorescence quantum yields of **PLB2** and **PLB3** in solution were even close to 1. **PLB1**, **PLB3**, **PLB4**, and **PLB6**, which displayed good luminescence properties in both the aggregated and dispersed states, have been utilized to fabricate LEDs. Two WLEDs have been successfully prepared by adjusting the chip and doping concentrations. These two devices based on **PLB4** had high luminous efficiencies (LE) and color rendering indices (CRIs). In comparison with commercial WLEDs, these two devices had some superior properties. In addition, four compounds were used to prepare blue, green, yellow, and near-infrared LED devices, all of which outperformed commercial LEDs to some extent. This work is informative for breaking through the limitations of existing LED materials.

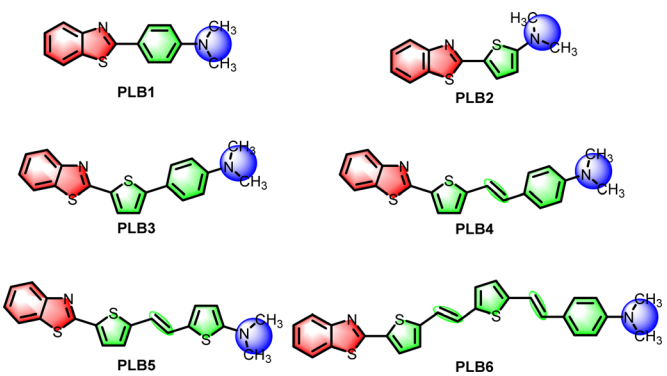


Scheme 1 Structure of target molecules **PLB1–PLB6**.

# Results and discussion

### Synthesis and characterization

The key reactions in the synthesis of these compounds are those for the construction of benzothiazoles and C=C double bonds (Scheme S1, ESI†). Benzothiazoles (**PLB1**, **PLB2**, and intermediates 2a and 2b) were constructed by acetal reactions between 2-aminothiophenol and aromatic aldehydes. Dimethyl sulfoxide was added as both an oxidizing agent and a solvent. Most of the reaction yields were relatively high, reaching 97.46% at best. For the construction of C=C double bonds (**PLB4–PLB6** and intermediate 8), we chose the Wittig reaction.[45] Yields were in the range 38.52–81.47%. Benzyl phosphite in the Wittig reaction is produced by the Arbuzov reaction. Intermediates 5 and 7 were obtained according to this protocol. Most of the aldehyde compounds were procured from suppliers. However, aldehyde intermediate 9 is produced by Bouveault aldehyde synthesis. **PLB3** was obtained by a Suzuki coupling reaction. All target molecules were characterized by $^{1}$H NMR, $^{13}$C NMR, and high-resolution mass spectrometry (Fig. S8–S31, ESI†).

### UV/Vis absorption

Experimentally, we observed that **PLB1** and **PLB2** were pale-yellow solids, **PLB3** and **PLB4** were yellow/orange solids, and **PLB5** and **PLB6** were red solids (Fig. S1, ESI†). Accordingly, we tentatively determined that **PLB1** and **PLB2** absorbed in the near-UV region (<400 nm), **PLB3** and **PLB4** absorbed in the blue region (around 450 nm), while **PLB5** and **PLB6** absorbed in the green region (around 520 nm). This was in line with the expectation that the absorption is gradually red-shifted as the π-bridge is extended. The UV/Vis absorption spectra of all six compounds in $CH_2Cl_2$ solution ($1 \times 10^{-5}$ mol $L^{-1}$) were recorded (Fig. 1). Each spectrum featured a strong absorption peak at around 265 nm and a weak absorption peak in the range of 290–350 nm. These absorption peaks could be mainly attributed to the $^{1}\pi$–$\pi^*$ transition. Each of the six compounds also showed a strong absorption peak in the range 350–500 nm, at 357 nm, 388 nm, 410 nm, 433 nm, 470 nm, and 475 nm for **PLB1–PLB6**, respectively. Evidently, the absorption peaks of the

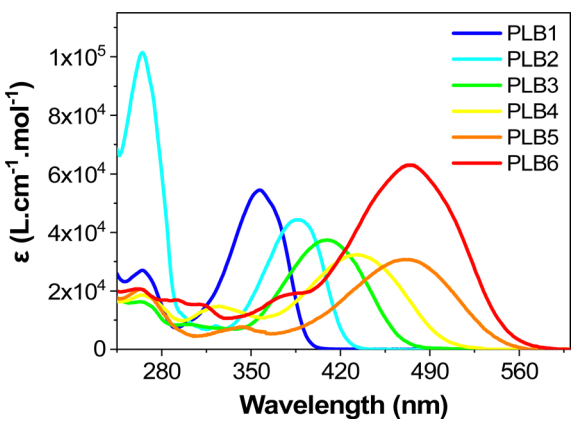


Fig. 1 The UV-vis absorbance spectra of **PLB1–PLB6** in $CH_2Cl_2$ solution ($1 \times 10^{-5}$ mol $L^{-1}$) measured at room temperature.

six compounds in this range were gradually red-shifted with extension of the π-bridge. Therefore, these absorption peaks were mainly attributed to intramolecular charge transfer (ICT). This was corroborated by the absorption spectra of the six compounds in different polar solvents. As shown in Fig. S2 (ESI†), the absorption peaks of the six compounds above 350 nm were gradually red-shifted with increasing solvent polarity, whereas the absorption peaks below 350 nm did not change significantly. A comparison of the absorption spectra of **PLB1** and **PLB2** revealed that the replacement of benzene by thiophene favored the absorption red-shift of these compounds. A similar conclusion was drawn by comparing **PLB4** and **PLB5**. Moreover, comparison of **PLB3** and **PLB4** revealed that the insertion of a double-bond unit also facilitated the absorption red-shift of these compounds. Comparing **PLB4** and **PLB6**, it can be found that the extension of the π bridge will greatly promote the redshift of absorption. The same conclusion can be drawn after comparing **PLB5** and **PLB6**. Therefore, π-bridge modification substantially modulated the absorption properties of these D–π–A compounds.

### Photoluminescence

The six compounds exhibited different luminescence colors in $CH_2Cl_2$ solution (Fig. 2d), namely blue-violet, blue, green, yellow, orange, and red, under irradiation with a UV lamp (365 nm). From the emission spectra of **PLB1–PLB6** in $CH_2Cl_2$ solution (Fig. 2a), their maximum emission wavelengths were determined to be 408 nm, 446 nm, 513 nm, 570 nm, 614 nm, and 638 nm, respectively (Table 1). This was consistent with the observed phenomena. To confirm their luminescence colors, we calculated the CIE (Commission Internationale de l'Eclairage) of the six compounds based on their emission spectra. As shown in Fig. 2b, the CIE of the six compounds in $CH_2Cl_2$ solution were evaluated as (0.16, 0.02), (0.15, 0.06), (0.24, 0.59), (0.47, 0.52), (0.59, 0.40), and (0.62, 0.38), respectively. The colors were consistent with the initial judgment. The spectra of the six compounds covered the whole visible region from blue to red. Moreover, the spectral region of **PLB6** included a certain near-infrared interval (>780 nm). This variation trend proved to be consistent with the absorption spectra. That is to say, the emission wavelength was gradually red-shifted with extension of the π-bridge. Therefore, we surmised that the luminescence of these compounds originated from intramolecular $^1\pi$–$\pi^*$ transitions and was accompanied by ICT processes.

Fluorescent molecules with ICT properties usually show a significant solvatochromic effect. We recorded the emission spectra of **PLB1–PLB6** in hexane, toluene, tetrahydrofuran, $CH_2Cl_2$, and acetonitrile, respectively (Fig. S3, ESI†). All six compounds showed a significant solvatochromic effect. Among them, **PLB3–PLB6** displayed rich color variations in all five solvents. **PLB3** showed a color variation from blue to yellow, while **PLB6** showed a color variation from green to red, as shown in the insets in Fig. 3. **PLB4** and **PLB5** also showed distinct color change effects (insets in Fig. S3d and e, ESI†). The emission wavelength variations of **PLB3–PLB6** in hexane and acetonitrile were 93 nm, 128 nm, 122 nm, and 149 nm,

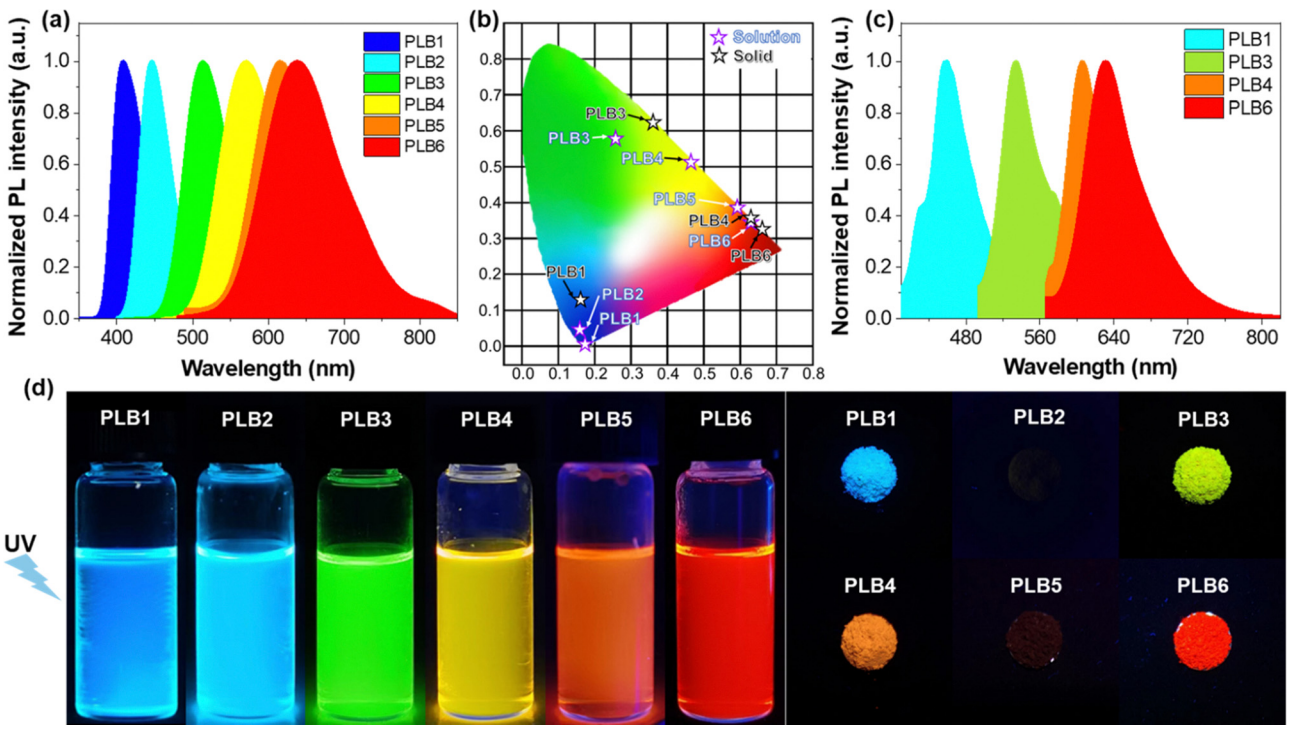


Fig. 2 (a) Photoluminescence spectra of **PLB1–PLB6** in $CH_2Cl_2$ solution ($1 \times 10^{-5}$ mol $L^{-1}$). (b) Chromaticity coordinate chart of the six compounds in $CH_2Cl_2$ solution ($1 \times 10^{-5}$ mol $L^{-1}$) and solid state. (c) Photoluminescence spectra of **PLB1**, **PLB3**, **PLB4**, and **PLB6** in the solid state. (d) Images of the six compounds in $CH_2Cl_2$ solution ($1 \times 10^{-5}$ mol $L^{-1}$) and solid state under the irradiation of a 365 nm UV-lamp.

 

Table 1 UV-visible absorption and photoluminescence parameters of **PLB1–PLB6** in $CH_2Cl_2$ solution (sol.) and solid powder (pow.)

| Cpd. | $\lambda_{abs}$/nm ($\varepsilon/10^4$ L mol$^{-1}$ cm$^{-1}$) | $\lambda_{ex}$/nm | | $\lambda_{em}$/nm | | Stokes shift/nm | | $\Phi_{em}$ | | $\tau$/ns | |
|---|---|---|---|---|---|---|---|---|---|---|---|
| | | Sol. | Pow. | Sol. | Pow. | Sol. | Pow. | Sol. | Pow. | Sol. | Pow. |
| **PLB1** | 265 (2.71), 357 (5.45) | 338 | 400 | 408 | 465 | 70 | 65 | 0.97 | 0.08 | 1.71 | 2.83 |
| **PLB2** | 265 (10.14), 322 (0.81), 388 (4.43) | 396 | — | 446 | — | 50 | — | 0.99 | — | 2.41 | — |
| **PLB3** | 265 (1.62), 300 (0.86), 410 (3.74) | 396 | 467 | 513 | 535 | 117 | 68 | 0.99 | 0.99 | 2.55 | 4.09 |
| **PLB4** | 264 (1.87), 326 (1.48), 433 (3.23) | 434 | 467 | 570 | 605 | 136 | 138 | 0.64 | 0.40 | 1.92 | 3.64 |
| **PLB5** | 264 (2.07), 345 (0.77), 470 (3.07) | 468 | — | 614 | — | 146 | — | 0.11 | — | 0.74 | — |
| **PLB6** | 263 (2.07), 291 (1.69), 475 (6.30) | 459 | 467 | 638 | 631 | 179 | 164 | 0.28 | 0.16 | 1.27 | 3.77 |

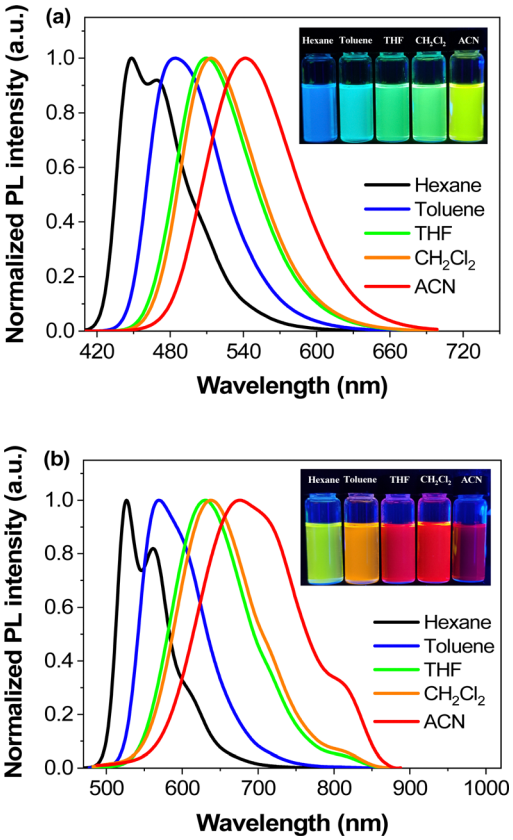


Fig. 3 Photoluminescence spectra of **PLB3** (a) and **PLB6** (b) in different polar solvents ($1 \times 10^{-5}$ mol L$^{-1}$) and luminescence images (inset) under the irradiation of a 365 nm UV-lamp.

respectively. Such variations make them valuable for applications in solvent probes[46–48] and biomarkers.[49] The observations were consistent with an increase in conjugation of the π-bridge promoting the ICT effect. Most of these compounds showed strong luminescence intensity. This was also evidenced by the measured fluorescence quantum yields (Table S1, ESI†). **PLB2** and **PLB3** were particularly notable for their dazzling luminescence. They both had fluorescence quantum yields close to 1. **PLB1**, **PLB4**, and **PLB6** also had bright luminescence, with fluorescence quantum yields of 0.965, 0.635, and 0.280 in $CH_2Cl_2$ solution, respectively. We found that the chosen highly polar solvents had a significant negative effect on the fluorescence quantum yields of **PLB1** and **PLB6**. This may be due to dipole–dipole interactions between the excited-state molecules and the solvent molecules.[50] Such interactions resulted in twisted intramolecular charge transfer (TICT), which in turn led to luminescence quenching.[51] The fluorescence quantum yield of **PLB5** in $CH_2Cl_2$ was only 0.11, whereas that of **PLB4**, which had a similar structure, was almost six times higher. This may be due to reductive quenching,[52] which was supported by electrochemical analysis (*vide infra*).

Compounds showing luminescence in the aggregated state are more convenient for application in LEDs. We found that four of the studied compounds, **PLB1**, **PLB3**, **PLB4**, and **PLB6**, maintained good luminescence in the solid state (Fig. 2d). The luminescence colors of the four compounds in the powder state were red, yellow, green, and blue, respectively. The emission peaks of **PLB1**, **PLB3**, **PLB4**, and **PLB6** were located at 513 nm, 570 nm, 614 nm, and 631 nm, respectively (Fig. 2c). This was consistent with the observed luminescent color of the powder, and the spectra of the four compounds covered the entire visible region. These compounds also exhibited panchromatic luminescence in the aggregated state. We compared the emission wavelengths of these four compounds in $CH_2Cl_2$ solution and in the aggregated state (Table 1). The results showed a significant variation in the emission of **PLB1** in the respective states. **PLB3** and **PLB4** also showed some variation, amounting to 22 nm and 35 nm, respectively, whereas **PLB6** showed almost no variation. This indicated that the radiative transitions of the two states are very similar. Therefore, the source of the luminescence in the aggregated state was also an intramolecular $^1\pi$–$\pi^*$ transition accompanied by an ICT process. The slight red-shift may be caused by vibrational relaxation due to intermolecular interactions.[53] Moreover, we found that **PLB3**, **PLB4**, and **PLB6** maintained luminescence in the aggregated state similar to that in the dispersed state, whereas luminescence in the aggregated state of **PLB1** was substantially attenuated. The luminescence of **PLB2** varied in the same way as that of **PLB1**. Its luminescence in the aggregated state was even completely quenched. From the data in Table 1, it was evident that the excitation wavelength of **PLB1** was relatively close to its emission wavelength, which meant that the emitted light re-excited other molecules. The probability of this occurring would be greater in the aggregated state, in which the distance between molecules was smaller.[54] Therefore, the attenuation of the luminescence of **PLB1** may be due to an insufficient Stokes shift. Photons released by the radiative transition were re-absorbed by other ground-state molecules and energy was gradually dissipated through several emission–absorption

cycles. The luminescence of **PLB2** in the aggregated state was similar to that of **PLB1**, and its Stokes shift was even smaller. Therefore, its luminescence in the aggregated state was more completely quenched. This phenomenon may also be caused by specific crystal stacking, which needs to be elaborated by crystal structure analysis. **PLB5** shows a large Stokes shift in solution, similar to those of **PLB4** and **PLB6**. Therefore, it may also maintain a large Stokes shift in the aggregated state, making secondary excitation less likely. In contrast, compounds with a strong ICT effect tend to have dipole–dipole interactions between molecules in the solid state,[55] thus suppressing the luminescence of the CT state. **PLB4** and **PLB6**, which are structurally similar to **PLB5**, also have weak luminescence decay.

### Theoretical calculations and electrochemistry

To further investigate the ground-state and low-level singlet-excited-state properties and their relationship with molecular structure, density functional theory (DFT) calculations were performed on **PLB1–PLB6** at the B3LYP/6-31G* level.[56,57] The ground-state geometries of **PLB1–PLB6** were fully optimized. The calculated results (Fig. 4) showed that the lowest unoccupied molecular orbital (LUMO) electron clouds of all six compounds had significant ICT compared to the highest occupied molecular orbitals (HOMOs). This phenomenon became increasingly pronounced with extension of the π-bridge. For example, the electron cloud of **PLB6** at the HOMO energy level was distributed over the π-bridge and dimethylamine group, with almost no electron density on the benzothiazole moiety. At the LUMO energy level, however, all electron density on the dimethylamine group and the connected benzene ring was transferred to the benzothiazole moiety. In contrast, only the electron density on the methyl group moved to the benzothiazole moiety when **PLB1** undergoes the transition. The energy gaps ($\Delta E_g$) between the HOMO and LUMO levels of the six compounds were evaluated as 3.95 eV, 3.57 eV, 3.10 eV, 2.78 eV, 2.62 eV, and 2.32 eV, respectively. Thus, $\Delta E_g$ decreased incrementally with extension of the π-bridge. This implied that for transitions between the HOMO and LUMO the corresponding absorption or emission wavelengths gradually increased with extension of the π-bridge. This was consistent with the results of UV absorption and photoluminescence studies.

We investigated the electrochemical properties of **PLB1–PLB6** by cyclic voltammetry. Cyclic voltammograms of these compounds are shown in Fig. 5. According to the literature, the HOMO and LUMO energy levels and energy gaps were estimated according to the following equations:[58,59]

$$E_{HOMO} = \left(-E^{ox}_{onset} + 4.4\right)\ \text{eV}$$

$$\Delta E_{gap} = 1240/\lambda_{edge}$$

$$E_{LUMO} = E_{HOMO} + \Delta E_{gap}$$

The electrochemical potentials and energy levels of the six compounds are shown in Table S2 (ESI†). It can be seen that with extension of the conjugated π-bridge, the HOMO energy levels of the six compounds gradually increased, while their energy gaps gradually decreased. This variation in trend is consistent with the results of the UV/Vis absorption and photoluminescence. Although the $E^{cal}_g$ values obtained from theoretical calculations (3.32–3.95 eV) were significantly higher than the $\Delta E_g$ values (2.25–3.16 eV) obtained from ground-state absorption and electrochemical calculations, the trend in the energy gaps of the compounds remained consistent. This difference most likely arose because the computational model was related to a vacuum environment, whereas the cyclic voltammograms and UV/Vis spectra were measured in solution. Notably, the onset oxidation potentials of structurally similar **PLB4** and **PLB5** were 1.15 V and 0.68 V, respectively. That of **PLB4** was significantly higher, such that **PLB5** was more susceptible to oxidation. This further supported the conjecture

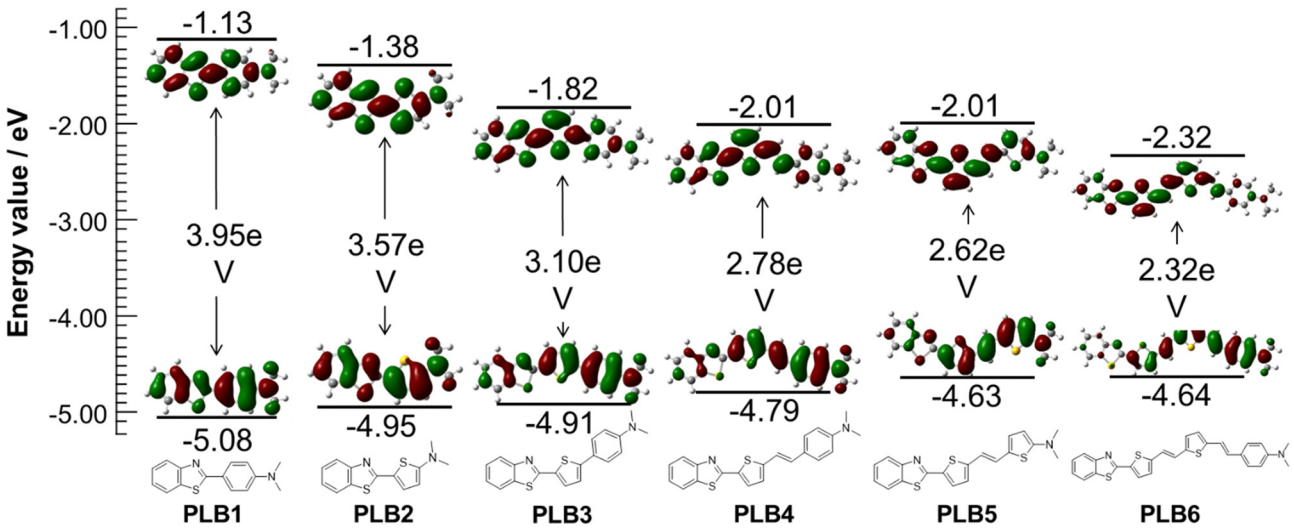


Fig. 4 Contour plots of electron density distribution and energy values of the HOMO and LUMO for **PLB1–PLB6**.

 

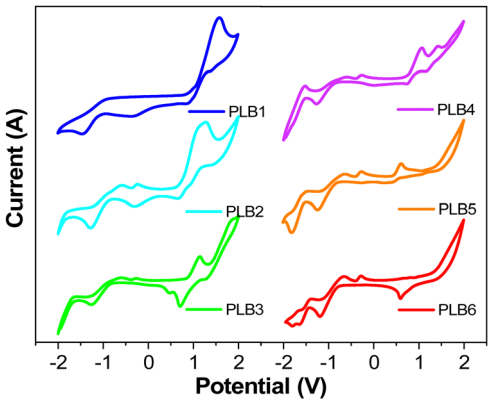


Fig. 5 The cyclic voltammograms of **PLB1**–**PLB6** ($1 \times 10^{-5}$ mol $L^{-1}$) in THF at 298.

that the low fluorescence quantum yield of **PLB5** was due to reductive quenching.[60]

### Crystal structure analysis

We analyzed single crystals of the compounds to further explore the relationship between intermolecular interactions and luminescence in the aggregated state. We only obtained single crystals of **PLB1–PLB4**, the crystal structures of which are shown in Fig. S4 (ESI†). The crystals of the four compounds were all orthogonal crystal systems, belonging to the space groups *Pbca*, $Pna2_1$, $Pna2_1$, and $P2_12_12_1$, respectively. The single-crystal parameters are shown in Table S3 (ESI†).

The molecular stacking structures of the four compounds are shown in Fig. 6. The molecules of **PLB1**, **PLB3**, and **PLB4** were mainly stacked in J-aggregation (misaligned stacking).[61,62] **PLB2** crystals had both J-aggregation and H-aggregation

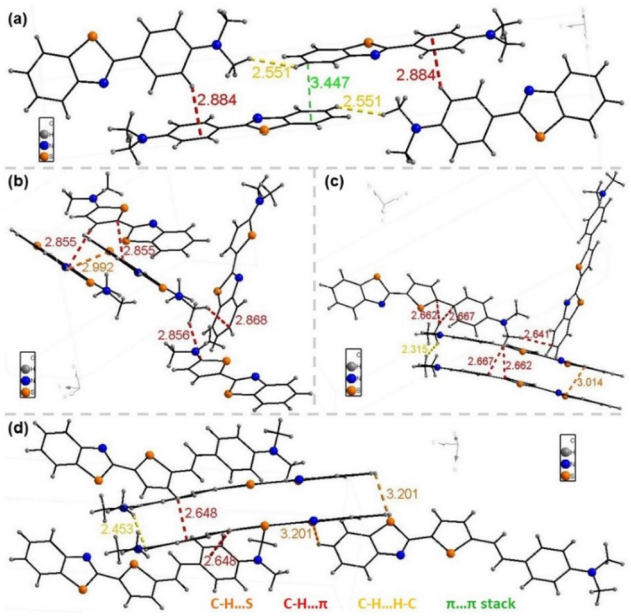


Fig. 6 The molecular stacking structure and interactions between molecules of (a) **PLB1**, (b) **PLB2**, (c) **PLB3**, and (d) **PLB4**.

(parallel stacking), in which two molecules in the H-aggregated state were stacked in a "face-to-edge" manner.[63] Both J-aggregation and the "face-to-edge" arrangement effectively prevented π–π stacking and thereby promoted intermolecular charge transfer. Such compounds can maintain their luminescent properties, and even show enhanced luminescence.[64,65] In addition, intermolecular interactions such as C–H···π were present in the crystals of all four compounds, with interaction distances greater than 2.5 Å. These interactions maintained a certain distance between molecules and prevented π–π stacking. In summary, the four molecules were stacked in a way that is favorable for luminescence in the aggregated state. **PLB3** and **PLB4** in the aggregated state maintained luminescence close to that in the dispersed state. However, **PLB1** and **PLB2** in the aggregated state showed significantly suppressed luminescence, and that of **PLB2** was even completely quenched. Therefore, we again determined that the reason for the suppressed luminescence in the aggregated state for these two compounds was that their Stokes shifts were too small. The light emitted by the radiative transition was absorbed by other ground-state molecules, and the energy is gradually dissipated after several emission/absorption cycles. In addition, there were intermolecular interactions such as C–H···π in all of the crystals, which led to vibrational relaxation.[53] This contributed to a weak red-shift of the solid-state luminescence compared to the dispersed state.

### Assembly of LED devices

**PLB1**, **PLB3**, **PLB4**, and **PLB6** have good luminescence properties in both the aggregated and dispersed states. Therefore, we prepared LED devices from these four compounds to demonstrate their luminescence properties and to verify their practicality. We chose the solution deposition method to prepare the LEDs by first dispersing the compounds in commercial A/B gel and then coating them on blue or UV LED chips. This process was more energy-efficient, environmentally friendly, and simple to operate, compared to the conventional vapor deposition method,[66,67] and it was suitable for small organic molecules. The fabrication of WLEDs required yellow/orange-emitting materials as the color conversion layer. **PLB3** and **PLB4** both had luminescent colors close to yellow, so they were chosen to prepare the WLEDs. LEDs with an emission wavelength of 450 nm were selected as the chips, which can excite both compounds while supplying the blue light component of the WLEDs. To tune the absorption/transmission ratio of the light source, devices with five different doping ratios were prepared to screen for the best WLED. The two compounds were then doped in A/B gel and coated on the chips. In this way, ten LED devices were successfully prepared. We also tried to fabricate full-color LEDs. Four LEDs with emission wavelengths of 365 nm, 395 nm, 425 nm, and 450 nm were selected as chips in devices based on the four compounds according to their optimal excitation wavelengths. They are named UV-365, UV-395, Blue-425, and Blue-450, accordingly. The four compounds have different luminescence properties in the aggregated and dispersed states. Therefore, we controlled the doping ratio to select the best LED devices. In total, 17 such LED devices were

prepared. For convenience of presentation, we numbered the above 27 devices in order of compound structure from small to large, doping concentration from high to low, and chip wavelength from short to long. The device appearances, luminescence effects, and doping amounts are summarized in Fig. S5 (ESI†). The photographs showed that the luminescence of **PLB3** and **PLB4** were close to white at a doping level of about 0.1. The emission spectra of all of the devices were measured (Fig. S6, ESI†), and their spectral parameters are collected in Table S4 (ESI†).

To determine the luminescence colors more accurately, we plotted the CIE of these devices (Fig. S7, ESI†). Devices 17 and 22, prepared from **PLB4** at a doping concentration of 0.1, fall in the white region on the chromaticity coordinate diagram. Their CIE were (0.37, 0.36) and (0.28, 0.27), respectively. Their emission spectra (Fig. 7) had a dual-emission structure covering the entire visible band. This further proved that it was white light emission. It is worth noting that their LE reached 115.81 lm $W^{-1}$ and 95.31 lm $W^{-1}$, respectively, far exceeding those of similar WLEDs. Their CRIs were evaluated as 60 and 80, respectively. The latter parameter was indicative of illumination that meets the requirement for color discrimination. Device 17 is a warm white LED, while device 22 is a cool white

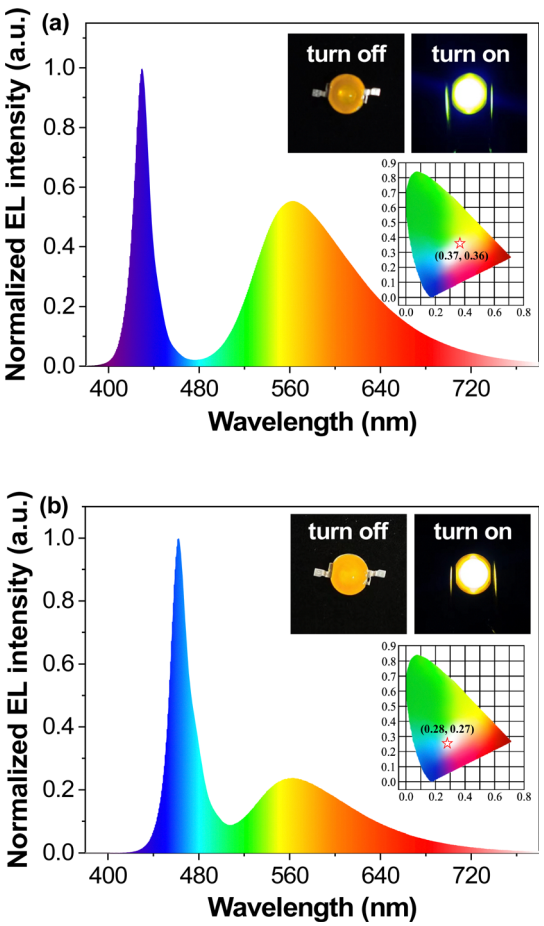


Fig. 7 Spectra, energized/unenergized photos (inset), and chromaticity coordinate chart (inset) of device 17 (a) and device 22 (b).

Table 2 The electroluminescent data of device 17, device 22, white1, and white2

| | CIE | CCT (K) | CRI | LE (lm $W^{-1}$) |
|---|---|---|---|---|
| Device 22 | (0.28, 0.27) | 11 580 | 80 | 95.31 |
| White1 | (0.28, 0.27) | 8397 | 78 | 109.52 |
| Device 17 | (0.37, 0.36) | 4290 | 60 | 115.81 |
| White2 | (0.37, 0.37) | 4160 | 63 | 122.79 |

LED, based on correlated color temperatures (CCT) of 4290 and 11 580, respectively. Warm light makes people relaxed, and so it is suitable for home and entertainment lighting, while cool light tends to make people more focused, and is suitable for work and study environments. Both devices had their strengths. To better illustrate the superiority of their properties, two commercial WLEDs were purchased for comparison. The properties of these commercial WLEDs were tested under the same conditions as the two LEDs mentioned above. The results are shown in Table 2 and Table S4 (ESI†). White1 was a cool white LED and white2 was a warm white LED. The CIE and LE of device 22 are very close to those of white1. And the CRI is slightly higher. The warm white device 17 closely resembled white2 in all parameters. Indeed, we found that the absorption/transmission ratio of the chip was perfectly suited for white light emission when the mass fraction of **PLB4** was around 9%. These devices with excellent performance may be considered valuable for commercial development.

**PLB3** was an extremely bright emitter, with a fluorescence quantum yield close to 1. Most devices prepared from it also have high luminescence efficiency, and most of them outperform commercial LEDs. **PLB3**-based device 11 gave a very good approximation of white light emission and had a higher LE than device 17. However, its color was greenish in terms of CIE (Fig. S7, ESI†), making it unsuitable for use in WLEDs. However, devices 4–6 and 9 prepared from it were yellow LEDs with a very high LE, and were significantly superior to commercial yellow LEDs (Table S4, entry 31, ESI†). Device 10 was a green LED, which also had high LE and is comparable to commercial green LEDs (Table S4, entry 30, ESI†). The luminescence efficiency of device 16 prepared from **PLB4** was also better than that of commercial yellow LEDs. **PLB1** was a molecule with high luminescence in the dispersed state, and the luminescence efficiency of device 1 prepared from it was much better than that of commercial blue LEDs (Table S4, entry 29, ESI†). Device 24, prepared from **PLB6**, was a near-infrared LED device. Overall, this series of panchromatic luminescent compounds may have good potential for application in panchromatic LEDs.

To further verify the practicality of these materials, the four compounds applied in LEDs were tested for thermal stability. Thermogravimetric analysis traces for **PLB1**, **PLB3**, **PLB4**, and **PLB6** are shown in Fig. 8. We have marked the temperatures at which the four materials maintained 95% of the original mass. The four compounds remained stable at temperatures of 210.0 °C, 298.8 °C, 287.7 °C, and 324.5 °C, respectively, showing them to have good thermal stability. In particular, **PLB3** and

 

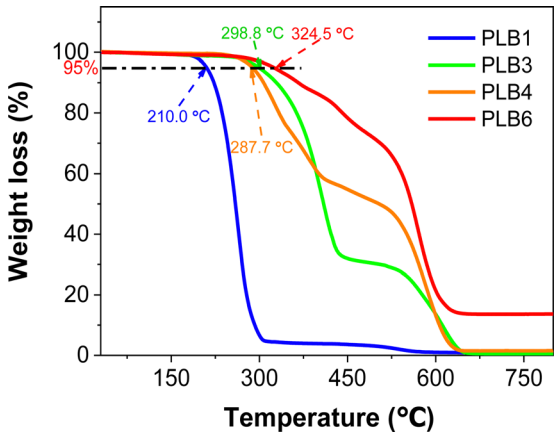


Fig. 8 Thermogravimetric analysis curve of **PLB1**, **PLB3**, **PLB4**, and **PLB6**. The five compounds are labeled at 95% mass temperature.

**PLB6** maintained good stability at around 300 °C. LED devices fabricated from these materials should thus show stable long-term luminescence.

## Conclusions

We have constructed D–π–A-type fluorescent small molecules using simple benzothiazole and dimethylamine as electron-donor and -acceptor groups, respectively. Six compounds with panchromatic luminescence were obtained by introducing benzene, thiophene, and C=C double-bond units to modulate the π-bridge length. The six compounds covered the entire visible spectrum, not only in solution, but also in the solid state. The conformational relationships of the compounds have been systematically investigated through photoluminescence spectroscopy, quantitative calculations, and single-crystal analysis. We found that incremental adjustment of the degree of conjugation of the bridging unit resulted in a series of compounds with significant variation in luminescence color. However, too long a π-bridge may lead to a decrease in fluorescence quantum yield. We used **PLB1**, **PLB3**, **PLB4**, and **PLB6**, which have good luminescence properties in both the aggregated and dispersed states, to fabricate LEDs. Two **PLB4**-based WLEDs were successfully prepared by adjusting the chip and doping concentrations. One was a warm WLED, while the other was a cool WLED. Their LEs were measured as 115.81 lm $W^{-1}$ and 95.31 lm $W^{-1}$, and their CRIs were evaluated as 60 and 80, respectively. Some of their properties exceeded those of commercial WLEDs. In addition, the four compounds were used to prepare blue, green, yellow, and near-infrared LEDs, all of which exceeded the performance of existing commercial LEDs to some extent. This research work was of reference value to break through the limitations of existing LED materials.

## Author contributions

Yuwei Song: methodology, data curation, writing – original draft; Zhiyuan Chen: data curation; Lai Hu: investigation; Qian Cheng: data curation; Yue He: conceptualization; Rui Liu: conceptualization, writing – review & editing, supervision; Senqiang Zhu: funding acquisition, supervision; Hongjun Zhu: funding acquisition, supervision.

## Conflicts of interest

The authors declare no competing financial interest.

## Acknowledgements

The authors greatly acknowledge the Natural Science Foundation of Jiangsu Province (BK20220351), the Natural Science Foundation of the Jiangsu Higher Education Institutions of China (22KJB150027), and the Postgraduate Research & Practice Innovation Program of Jiangsu Province (KYCX22-1277). The computational resources generously provided by the High Performance Computing Center of Nanjing Tech University are greatly appreciated.

## References

1 H. Zhang, H. Zhang and A. Pan, *et al.*, Rare Earth-Free Luminescent Materials for WLEDs: Recent Progress and Perspectives, *Adv. Mater. Technol.*, 2021, **6**(1), 2000648.
2 L. Kang and Z. Lin, Regulation strategy of white emission from organic–inorganic hybrid metal halide perovskites, *Inorg. Chem. Front.*, 2023, **10**, 13–36.
3 Y.-S. Park, J.-W. Kang and D. M. Kang, *et al.*, Efficient, Color Stable White Organic Light-Emitting Diode Based on High Energy Level Yellowish-Green Dopants, *Adv. Mater.*, 2008, **20**(10), 1957–1961.
4 J. Y. Tsao, M. H. Crawford and M. E. Coltrin, *et al.*, Toward Smart and Ultra-efficient Solid-State Lighting, *Adv. Opt. Mater.*, 2014, **2**(9), 809–836.
5 H. Peng, X. He and Q. Wei, *et al.*, Realizing High-Efficiency Yellow Emission of Organic Antimony Halides via Rational Structural Design, *ACS Appl. Mater. Interfaces*, 2022, **14**(40), 45611–45620.
6 R. Dong, D. Liu and J. Li, *et al.*, Acceptor modulation for blue and yellow TADF materials and fabrication of all-TADF white OLED, *Mater. Chem. Front.*, 2022, **6**(1), 40–51.
7 J. Chatsirisupachai, P. Nalaoh and C. Kaiyasuan, *et al.*, Unique dual fluorescence emission in the solid state from a small molecule based on phenanthrocarbazole with an AIE luminogen as a single-molecule white-light emissive material, *Mater. Chem. Front.*, 2021, **5**(5), 2361–2372.
8 W. Han, S.-H. Chae, T. Kim, D. Lee and H. Kim, White-light-emitting triphasic fibers as a phosphor for light-emitting diodes, *Nanoscale Adv.*, 2020, **2**(11), 5403–5411.
9 A. B. Kajjam, P. S. V. Kumar, V. Subramanian and S. Vaidyanathan, Triphenylamine based yellowish-orange light emitting organic dyes (donor–π–acceptor) for hybrid WLEDs and OLEDs: synthesis, characterization and theoretical study, *Phys. Chem. Chem. Phys.*, 2018, **20**(6), 4490–4501.

10 Q. Wang, J. Ding and D. Ma, *et al.*, Manipulating Charges and Excitons within a Single-Host System to Accomplish Efficiency/CRI/Color-Stability Trade-off for High-Performance OWLEDs, *Adv. Mater.*, 2009, **21**(23), 2397–2401.
11 H. Yuce, T. Guner and S. Dartar, *et al.*, BODIPY-based organic color conversion layers for WLEDs, *Dyes Pigm.*, 2020, **173**, 107932.
12 N. Yang, Z. Zhang and L. Zou, *et al.*, A novel red-emitting phosphor with an unusual concentration quenching effect for near-UV-based WLEDs, *Inorg. Chem. Front.*, 2022, **9**(24), 6358–6368.
13 Q. Chang, T. Ma, C. Liu, J. Hu and X. Cheng, Benzo[1,2-*b*:4,3-*b*′]dithiophene-pyridine isomers: Synthesis, self-assembly, photophysical and acidochromic properties, *Dyes Pigm.*, 2022, **205**, 110490.
14 D. Luo, Y. Yang and Y. Xiao, *et al.*, Regulating Charge and Exciton Distribution in High-Performance Hybrid White Organic Light-Emitting Diodes with n-Type Interlayer Switch, *Nano-Micro Lett.*, 2017, **9**(4), 37.
15 B.-Q. Liu, L. Wang and D.-Y. Gao, *et al.*, Extremely high-efficiency and ultrasimplified hybrid white organic light-emitting diodes exploiting double multifunctional blue emitting layers, *Light: Sci. Appl.*, 2016, **5**(8), 16137.
16 B. Liu, H. Nie and X. Zhou, *et al.*, Manipulation of Charge and Exciton Distribution Based on Blue Aggregation-Induced Emission Fluorophors: A Novel Concept to Achieve High-Performance Hybrid White Organic Light-Emitting Diodes, *Adv. Funct. Mater.*, 2016, **26**(5), 776–783.
17 S. Pimputkar, J. S. Speck, S. P. DenBaars and S. Nakamura, Prospects for LED lighting, *Nat. Photonics*, 2009, **3**, 180–182.
18 B. Li, D. Zhang and Y. Li, *et al.*, A reversible vapor-responsive fluorochromic molecular platform based on coupled AIE–ESIPT mechanisms and its applications in anti-counterfeiting measures, *Dyes Pigm.*, 2020, **181**, 108535.
19 Y. Yamaguchi, T. Ochi, Y. Matsubara and Z. Yoshida, Highly Emissive Whole Rainbow Fluorophores Consisting of 1,4-Bis(2-phenylethynyl)benzene Core Skeleton: Design, Synthesis, and Light-Emitting Characteristics, *J. Phys. Chem. A*, 2015, **119**(32), 8630–8642.
20 D. Li, H. Zhang and C. Wang, *et al.*, Construction of full-color-tunable and strongly emissive materials by functionalizing a boron-chelate four-ring-fused π-conjugated core, *J. Mater. Chem.*, 2012, **22**(10), 4319–4328.
21 Y. Chen, Y. Fang and H. Gu, *et al.*, Color-Tunable and ESIPT-Inspired Solid Fluorophores Based on Benzothiazole Derivatives: Aggregation-Induced Emission, Strong Solvatochromic Effect, and White Light Emission, *ACS Appl. Mater. Interfaces*, 2020, **12**(49), 55094–55106.
22 S. Ji, Z. Ding, J. Zhao and D. Zheng, Substituent control of dynamical process for excited state intramolecular proton transfer of benzothiazole derivatives, *Chem. Phys.*, 2022, **560**, 111568.
23 D. Göbel, P. Rusch and D. Duvinage, *et al.*, Substitution Effect on 2-(Oxazolinyl)-phenols and 1,2,5-Chalcogenadiazole – Annulated Derivatives: Emission-Color-Tunable, Minimalistic Excited-State Intramolecular Proton Transfer (ESIPT)-Based Luminophores, *J. Org. Chem.*, 2021, **86**(21), 14333–14355.
24 M. Tian, J. Sun, B. Dong and W. Lin, Dynamically Monitoring Cell Viability in a Dual-Color Mode: Construction of an Aggregation/Monomer-Based Probe Capable of Reversible Mitochondria-Nucleus Migration, *Angew. Chem., Int. Ed.*, 2018, **57**(50), 16506–16510.
25 L. Wang, H. Zheng and K. Zheng, *et al.*, π-Expanded benzothiazole dyes with excited-state intramolecular proton-transfer process: Synthesis, photophysical properties, imaging in cells and zebrafish, *J. Mol. Liq.*, 2021, **344**, 117753.
26 D. Göbel, P. Rusch, D. Duvinage, N. C. Bigall and B. J. Nachtsheim, Emission color-tunable oxazol(in)yl-substituted excited-state intramolecular proton transfer (ESIPT)-based luminophores, *Chem. Commun.*, 2020, **56**(98), 15430–15433.
27 Y. Shi, R. B. M. Hill and J.-H. Yum, *et al.*, A High-Efficiency Panchromatic Squaraine Sensitizer for Dye-Sensitized Solar Cells, *Angew. Chem., Int. Ed.*, 2011, **50**(29), 6619–6621.
28 Z. Lei, C. Sun and P. Pei, *et al.*, Stable, Wavelength-Tunable Fluorescent Dyes in the NIR-II Region for In Vivo High-Contrast Bioimaging and Multiplexed Biosensing, *Angew. Chem., Int. Ed.*, 2019, **58**(24), 8166–8171.
29 M. Zhao, B. Li and Y. Wu, *et al.*, A Tumor-Microenvironment-Responsive Lanthanide–Cyanine FRET Sensor for NIR-II Luminescence-Lifetime In Situ Imaging of Hepatocellular Carcinoma, *Adv. Mater.*, 2020, **32**(28), 2001172.
30 W. Fu, C. Yan and Z. Guo, *et al.*, Rational Design of Near-Infrared Aggregation-Induced-Emission-Active Probes: In Situ Mapping of Amyloid-β Plaques with Ultrasensitivity and High-Fidelity, *J. Am. Chem. Soc.*, 2019, **141**(7), 3171–3177.
31 A. Shao, Y. Xie and S. Zhu, *et al.*, Far-Red and Near-IR AIE-Active Fluorescent Organic Nanoprobes with Enhanced Tumor-Targeting Efficacy: Shape-Specific Effects, *Angew. Chem., Int. Ed.*, 2015, **54**(25), 7275–7280.
32 N. J. Findlay, J. Bruckbauer and A. R. Inigo, *et al.*, An Organic Down-Converting Material for White-Light Emission from Hybrid LEDs, *Adv. Mater.*, 2014, **26**(43), 7290–7294.
33 Y. Chen, W. Li and R.-Z. Gao, *et al.*, Covalent organic polymers with solid-state dual-color fluorescence tunable by ultraviolet irradiation, *J. Mater. Chem. C*, 2022, **10**(4), 1236–1245.
34 X. Li, H. Tang and L. Gao, *et al.*, A sp2-carbon-linked covalent organic framework containing tetraphenylethene units used as yellow phosphors in white light-emitting diodes, *Polymer*, 2022, **241**, 124474.
35 B. Vidya, M. Iniya, G. Sivaraman, R. V. Sumesh and D. Chellappa, Diverse benzothiazole based chemodosimeters for the detection of cyanide in aqueous media and in HeLa cells, *Sens. Actuators, B*, 2017, **242**, 434–442.
36 V. Botti, A. Cesaretti and Ž. Ban, *et al.*, Fine structural tuning of styryl-based dyes for fluorescence and CD-based sensing of various ds-DNA/RNA sequences, *Org. Biomol. Chem.*, 2019, **17**(35), 8243–8258.

 

37 S.-H. Chen, K. Jiang and J.-Y. Lin, *et al.*, Rational design and synthesis of Y-shaped fluorophores with multifarious emission properties and their application in the sensitive detection of PA, *J. Mater. Chem. C*, 2020, **8**(24), 8257–8267.
38 P. Alam, W. He and N. L. C. Leung, *et al.*, Red AIE-Active Fluorescent Probes with Tunable Organelle-Specific Targeting, *Adv. Funct. Mater.*, 2020, **30**(10), 1909268.
39 C. Shi, Z. Guo and Y. Yan, *et al.*, Self-Assembly Solid-State Enhanced Red Emission of Quinolinemalononitrile: Optical Waveguides and Stimuli Response, *ACS Appl. Mater. Interfaces*, 2013, **5**(1), 192–198.
40 M. Ono, S. Hayashi and H. Kimura, *et al.*, Push–pull benzothiazole derivatives as probes for detecting β-amyloid plaques in Alzheimer's brains, *Bioorg. Med. Chem.*, 2009, **17**(19), 7002–7007.
41 Y. Wei, X. Hu and L. Shen, *et al.*, Dicyanomethylene Substituted Benzothiazole Squaraines: The Efficiency of Photodynamic Therapy In Vitro and In Vivo, *EBioMedicine*, 2017, **23**, 25–33.
42 A. Ekbote, S. M. Mobin and R. Misra, Structure–property relationship in multi-stimuli responsive D–A–A′ benzothiazole functionalized isomers, *J. Mater. Chem. C*, 2018, **6**(40), 10888–10901.
43 K. Takahashi, K. Sambe and Y. Kasahara, *et al.*, Solid-State Fluorescence of Excited-State Cation–Anion Intermolecular Proton Transfer in 2-(2-Hydroxypyridyl)benzothiazole, *Adv. Opt. Mater.*, 2022, **10**(11), 2200134.
44 Y. Song, L. Hu and Q. Cheng, *et al.*, Benzothiazole derivatives with varied π-conjugation: synthesis, tunable solid-state emission, and application in single-component LEDs, *J. Mater. Chem. C*, 2022, **10**(16), 6392–6401.
45 R. D. A. Hudson, A. R. Manning and J. F. Gallagher, *et al.*, Chiral organometallic chromophores for nonlinear optics derived from $[Fe_2(h_5\text{-}C_5H_5)_2(CO)_2(m\text{-}CO)(m\text{-}C\text{-}/CH_3)]$ + $[BF_4]^-$, *J. Organomet. Chem.*, 2002, **655**, 70–88.
46 E. Benedetti, L. S. Kocsis and K. M. Brummond, Synthesis and Photophysical Properties of a Series of Cyclopenta[*b*]naphthalene Solvatochromic Fluorophores, *J. Am. Chem. Soc.*, 2012, **134**(30), 12418–12421.
47 T. Kuwabara, J. Orii, Y. Segawa and K. Itami, Curved Oligophenylenes as Donors in Shape-Persistent Donor-Acceptor Macrocycles with Solvatofluorochromic Properties, *Angew. Chem., Int. Ed.*, 2015, **54**(33), 9646–9649.
48 C.-H. Lim, M. D. Ryan and B. G. McCarthy, *et al.*, Intramolecular Charge Transfer and Ion Pairing in *N,N* -Diaryl Dihydrophenazine Photoredox Catalysts for Efficient Organocatalyzed Atom Transfer Radical Polymerization, *J. Am. Chem. Soc.*, 2017, **139**(1), 348–355.
49 H. Appelqvist, K. Stranius, K. Börjesson, K. Peter, R. Nilsson and C. Dyrager, Specific Imaging of Intracellular Lipid Droplets Using a Benzothiadiazole Derivative with Solvatochromic Properties, *Bioconjugate Chem.*, 2017, **28**(5), 1363–1370.
50 M. Kasha, H. R. Rawls and M. Ashraf El-Bayoumi, The exciton model in molecular spectroscopy, *Pure Appl. Chem.*, 1965, **11**(3–4), 371–392.
51 S. Kothavale and N. Sekar, Methoxy supported, deep red emitting mono, bis and tris triphenylamine-isophorone based styryl colorants: Synthesis, photophysical properties, ICT, TICT emission and viscosity sensitivity, *Dyes Pigm.*, 2017, **136**, 116–130.
52 G. Qian, Z. Zhong and M. Luo, *et al.*, Simple and Efficient Near-Infrared Organic Chromophores for Light-Emitting Diodes with Single Electroluminescent Emission above 1000 nm, *Adv. Mater.*, 2009, **21**(1), 111–116.
53 G. M. Stewart and J. D. McDonald, Intramolecular vibrational relaxation from C–H stretch fundamentals, *J. Chem. Phys.*, 1983, **78**(6), 3907–3915.
54 J. Kumsampao, C. Chaiwai and C. Sukpattanacharoen, *et al.*, Self-absorption-free excited-state intramolecular proton transfer (ESIPT) emitters for high brightness and luminous efficiency organic fluorescent electroluminescent devices, *Mater. Chem. Front.*, 2021, **5**(16), 6212–6225.
55 R. Bao, C. Zhang and Z. Wang, *et al.*, Large-Scale Controllable Patterning Growth of Aligned Organic Nanowires through Evaporation-Induced Self-Assembly, *Chem. – Eur. J.*, 2012, **18**(3), 975–980.
56 J. Lu, S. Zhu and H. Su, *et al.*, Synthesis, luminescence and excited state absorption properties of conjugated D-π-A and D-π-D phenothiazine compounds, *J. Lumin.*, 2019, **205**, 158–166.
57 H. Su, R. Liu and M. Shu, *et al.*, Fluorenone-based organogel and self-assembled fibrous film: Synthesis, optical properties and reversible detection of aniline vapor, *Dyes Pigm.*, 2019, **162**, 52–58.
58 Q. Sun, H. Wang, C. Yang and Y. Li, Synthesis and electroluminescence of novel copolymers containing crown ether spacers, *J. Mater. Chem.*, 2003, **13**(4), 800–806.
59 J. Wang, S. Zhu and R. Liu, *et al.*, Cyclometalated iridium(III) complex containing indolinyl-based phenanthroline ligand: Synthesis, structure and photophysical properties, *Inorg. Chim. Acta*, 2019, **491**, 132–137.
60 M. Velusamy, K. R. J. Thomas, J. T. Lin and Y. S. Wen, Benzo[1,2,5]selenadiazole bridged amines: electro-optical properties, *Tetrahedron Lett.*, 2005, **46**(44), 7647–7651.
61 T. Zhou, F. Li and Y. Fan, *et al.*, Hydrogen-bonded dimer stacking induced emission of aminobenzoic acid compounds, *Chem. Commun.*, 2009, 3199.
62 S. Hisamatsu, H. Masu, M. Takahashi and K. Kishikawa, S. Kohmoto. Pairwise Packing of Anthracene Fluorophore: Hydrogen-Bonding-Assisted Dimer Emission in Solid State, *Cryst. Growth Des.*, 2015, **15**(5), 2291–2302.
63 J. Cornil, D. Beljonne, J.-P. Calbert and J.-L. Brédas, Interchain Interactions in Organic π-Conjugated Materials: Impact on Electronic Structure, Optical Response, and Charge Transport, *Adv. Mater.*, 2001, **13**(14), 1053–1067.
64 H. Lu, Y. Zheng and X. Zhao, *et al.*, Highly Efficient Far Red/Near-Infrared Solid Fluorophores: Aggregation-Induced Emission, Intramolecular Charge Transfer, Twisted Molecular Conformation, and Bioimaging Applications, *Angew. Chem., Int. Ed.*, 2016, **55**(1), 155–159.

65 A. Yoshida, M. Ikeshita, N. Komiya and T. Naota, Solid-state fluorescence of zwitterionic imidazolium pyridinolates bearing long alkyl chains: Control of emission properties based on variation of lamellar alignment, *Tetrahedron*, 2017, **73**(41), 6000–6007.
66 D. Wu, W. Gong and H. Yao, *et al.*, Highly efficient solid-state emission of diphenylfumaronitriles with full-color AIE, and application in explosive sensing, data storage and WLEDs, *Dyes Pigm.*, 2020, **172**, 107829.
67 X. Zheng, Y. Huang and D. Xiao, *et al.*, Space conjugation induced white light and room-temperature phosphorescence from simple organic small molecules: single-component WLED driven by both UV and blue chips, *Mater. Chem. Front.*, 2021, **5**(18), 6960–6968.



 